New Journal of Physics
The open-access journal for physics

Time-resolved qubit readout via nonlinear Josephson inductance

Georg M Reuther[1,5], David Zueco[2,3], Peter Hänggi[1] and Sigmund Kohler[4]

[1] Institut für Physik, Universität Augsburg, Universitätsstraße 1, D-86135 Augsburg, Germany
[2] Instituto de Ciencia de Materiales de Aragón y Departamento de Física de la Materia Condensada, CSIC-Universidad de Zaragoza, E-50009 Zaragoza, Spain
[3] Fundación ARAID, Paseo María Agustín 36, 50004 Zaragoza, Spain
[4] Instituto de Ciencia de Materiales de Madrid, CSIC, Cantoblanco, E-28049 Madrid, Spain
E-mail: georg.reuther@physik.uni-augsburg.de

New Journal of Physics **13** (2011) 093022 (19pp)
Received 5 May 2011
Published 12 September 2011
Online at http://www.njp.org/
doi:10.1088/1367-2630/13/9/093022

Abstract. We propose a generalization of dispersive qubit readout that provides the time evolution of a flux qubit observable. Our proposal relies on the nonlinear coupling of the qubit to a harmonic oscillator with high frequency, representing a dc superconducting quantum interference device. Information about the qubit dynamics is obtained by recording the oscillator response to resonant driving and subsequent lock-in detection. The measurement process is simulated for the example of coherent qubit oscillations. This corroborates the underlying measurement relation and also reveals that the measurement scheme possesses low backaction and high fidelity.

[5] Author to whom any correspondence should be addressed.

Contents

1. Introduction

The question of how to gain information about the state of a quantum system has intrigued researchers since the early days of quantum mechanics. With the advent of quantum computation, this fundamental question also became of practical interest, mainly because the final stage of a quantum algorithm is necessarily qubit readout. This task only requires distinguishing between two particular qubit states and thus can be achieved by projective measurements. Nevertheless, going beyond readout is of interest as well, since one also desires direct experimental evidence for coherent superpositions emerging, e.g., from tunnelling oscillations.

In order to obtain a quantum mechanical description of a measurement process, one usually models the measurement apparatus as a macroscopic quantum environment, i.e., as a heat bath, where the pointer of the apparatus corresponds to an effective bath coordinate. When interacting with the central quantum system, the bath acquires information about the system state. Owing to the macroscopic nature of the bath, one may assume that a fraction of the bath already possesses full information about the effective pointer coordinate [1]. Therefore one can obtain knowledge of the pointer position without violating fundamental laws of quantum mechanics.

In recent years, superconducting quantum circuits have provided a new arena to test fundamental questions of quantum mechanics in the laboratory. Prominent examples are the demonstration of coherent time evolution in charge qubits [2] and of Berry phases [3], as well as testing Bell inequalities [4]. Above all, different protocols for quantum measurement were successfully implemented in circuit quantum electrodynamics [5–8]. For a superconducting solid-state qubit, the practical measurement of one of its coordinates is carried out by

coupling it to a macroscopic environment, as given by external circuitry, via a quantum point contact [9, 10] or a harmonic oscillator. Depending on the setup, the oscillator is realized by a dc superconducting quantum interference device (SQUID) [11] or a superconducting resonator [12]. In both cases, the resonance frequency of the oscillator depends on the qubit state. Consequently, the response of the oscillator to a close-to-resonant ac excitation possesses a phase shift that can be measured and from which one can infer the qubit state. The first experiments in this direction worked with an oscillator whose frequency was much lower than the qubit splitting [5, 13, 14]. More recent experiments [6, 15] operated in the so-called dispersive regime, where the oscillator frequency and the qubit splitting are of the same order, while their detuning is still larger than their mutual coupling strength. A crucial detail is that the oscillator frequency and bandwidth naturally limit the time resolution in such qubit measurements. Thus, using the said schemes with slow oscillators, it is only possible to extract time-averaged information about the qubit state in general, but there is no possibility to resolve its dynamics in time.

Recently, a first step towards a time-resolved measurement of qubit dynamics was proposed [16, 17]: when a weak high-frequency field acts directly on the qubit, the reflected signal acquires a time-dependent phase shift by harmonic mixing. Lock-in amplification of the reflected signal then allows the obtaining of information about the qubit dynamics. In this paper, we combine both approaches and extend the scheme of [16, 17] to a qubit coupled to a driven high-frequency oscillator. A measurement protocol for such a setup is particularly appealing because an oscillation mode is part of most of the recent superconducting qubit designs. Moreover, the oscillator serves as a filter for quantum noise and thus reduces qubit decoherence. Here, we focus on a flux qubit embraced by a dc SQUID, whose fundamental frequency may even be tunable to some extent [18, 19]. As a particular feature of this realization, the qubit–oscillator coupling is nonlinear in the oscillator coordinate; that is, the coupling possesses both significant linear and quadratic contributions. It will turn out that for realistic parameters, the measurement scheme relies on the quadratic part of the coupling.

The paper is structured as follows. In section 2, we introduce our model and discuss dispersive qubit readout in generalized terms. The central relation on which our measurement scheme relies is derived in section 3. Section 4 is devoted to numerical studies in which we test our measurement relation and work out quantitatively measurement fidelity and backaction. Furthermore, we provide an estimate of the signal-to-noise ratio and discuss realistic parameters for a possible experimental implementation. The appendix contains details of the derivation of the measurement relation, the input–output formalism [20] and the Bloch–Redfield master equation that we use for obtaining numerical results.

2. Dissipative qubit–oscillator model

2.1. System–bath model

We consider a superconducting flux qubit coupled to a SQUID [7], as sketched in figure 1. The SQUID is modelled as a harmonic oscillator, which gives rise to the Hamiltonian [6, 7, 18, 21]

$$\mathcal{H}_0 = \frac{\hbar\omega_{\rm qb}}{2}\sigma_z + \hbar\Omega\,(a^\dagger a + \tfrac{1}{2}) + \hbar(\sigma_z\cos\theta - \sigma_x\sin\theta)[g_1(a+a^\dagger) + g_2(a+a^\dagger)^2]. \tag{1}$$

The first term represents the qubit with energy splitting $\hbar\omega_{\rm qb} = \hbar(\epsilon^2+\delta^2)^{1/2}$ and the mixing angle $\theta = \arctan(\delta/\epsilon)$, which depends on the controllable qubit bias energy ϵ and the qubit gap

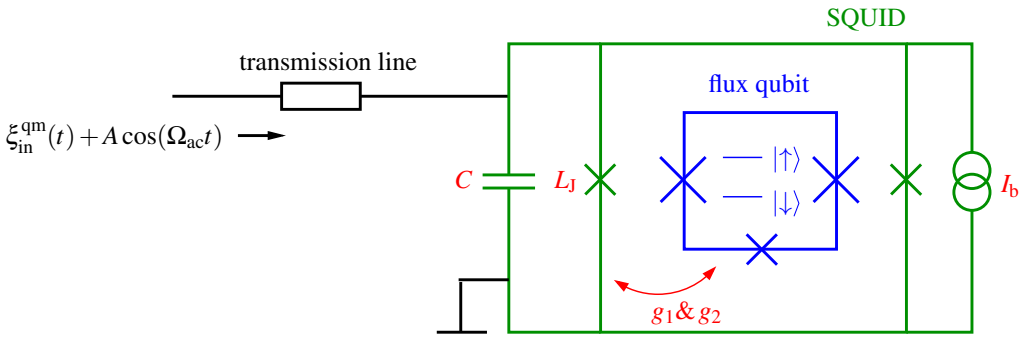

Figure 1. Sketch of the flux qubit (blue) coupled to a dc SQUID. The interaction is characterized by the linear coupling g_1, which depends linearly on the SQUID bias current $I_{\rm b}$ and the quadratic coupling g_2. The SQUID with Josephson inductance $L_{\rm J}$ is shunted by a capacitance C. The frequency shift of the resulting harmonic oscillator (green) can be probed by external resonant ac excitation $A\cos(\Omega_{\rm ac}t)$ via the transmission line (black), in which the quantum fluctuations $\xi_{\rm in}^{\rm qm}(t)$ are also present.

energy δ, while $\sigma_{x,z}$ denote the Pauli matrices. The second term describes the oscillator with frequency Ω and the bosonic creation and annihilation operators $a^\dagger$ and a, respectively. The qubit couples to the oscillator in two ways. First, via dipole interaction with strength g_1, which is linear in the oscillator coordinate $a+a^\dagger$. Up to order g_1^2, this causes a frequency shift for both the oscillator and the qubit. The second coupling term proportional to g_2, by contrast, is quadratic in the oscillator coordinate. Its physical origin is a nonlinear Josephson inductance, which depends on the magnetic flux, by which the SQUID is penetrated [7, 18]. This term provides a frequency shift already in first order of g_2. The interaction coefficients g_1 and g_2 can be controlled to some extent, as an expansion of the qubit–SQUID interaction to second order in the oscillator coordinate demonstrates [18]. In detail, for a small SQUID bias current $I_{\rm b}$, the coupling coefficient g_1 depends linearly on $I_{\rm b}$, whereas g_2 is independent of the latter, as we discuss in section 4.4. For $I_{\rm b}=0$, one even obtains $g_1=0$, such that the qubit couples only to the square of the oscillator position [7, 18].

Regarding a time-resolved measurement of the qubit dynamics via the oscillator, it will turn out that for realistic parameters of flux qubits, this quadratic coupling is crucial, while the linear coupling turns out to be typically too weak. For common circuit-QED setups using charge and flux qubits coupled to a transmission line resonator [11, 12, 22, 23], not only g_1 but also g_2 is too small. Thus, we henceforth focus on setups of flux qubits coupled to SQUIDs possessing a sizable quadratic coupling, as described above.

The qubit–SQUID system is further coupled to external circuitry, which acts as a dissipative environment and is modelled by the system–bath Hamiltonian [24–27]

$$\mathcal{H}=\mathcal{H}_0+Q\sum_k \hbar c_k(b_k+b_k^\dagger)+\sum_k \hbar\omega_k(b_k^\dagger b_k+\tfrac{1}{2}). \tag{2}$$

Here, $Q=a^\dagger+a$ is the oscillator coordinate, such that the interaction term represents the inductive coupling between the qubit and the flux degree of freedom of the SQUID. The system–bath interaction can be fully characterized by the spectral density $J(\omega)=\pi\sum_k|c_k|^2\delta(\omega-\omega_k)$, which is proportional to the real part of the effective impedance of

the environment [28]. Here we assume an ohmic spectral density, $J(\omega) = \alpha\omega$, for which the dimensionless damping strength α can be interpreted as effective resistance [29–31].

2.2. *Qubit–oscillator interaction in the dispersive limit*

We are interested in the dispersive limit, which is characterized by a detuning $\Delta = \Omega - \omega_{\rm qb}$ larger than the qubit–oscillator couplings,

$$g_1, g_2 \ll |\Delta|, \quad \Delta = \Omega - \omega_{\rm qb}. \tag{3}$$

It is then convenient to go to the dispersive picture via the unitary transformation (A.2). As detailed in appendix A, this yields the effective Hamiltonian [32, 33]

$$\bar{\mathcal{H}}_0 = \mathcal{U}^\dagger \mathcal{H}_0 \mathcal{U} = \hbar\bar{\Omega}(\bar{a}^\dagger \bar{a} + \tfrac{1}{2}) + \frac{\hbar\omega_{\rm qb}}{2}\sigma_z, \tag{4}$$

where the transformed bosonic operators $\bar{a}$ and $\bar{a}^\dagger$ are defined in equation (A.10). The qubit–oscillator coupling has been removed formally by shifting it to the operator-valued oscillator frequency

$$\bar{\Omega} = \Omega\sqrt{1 + \frac{4\bar{\omega}}{\Omega}}, \tag{5}$$

where the overbar denotes the dispersive picture, while the qubit operator

$$\bar{\omega} = \frac{g_1^2}{2}\sigma_z\left(\frac{1}{\Delta} - \frac{1}{\Omega + \omega_{\rm qb}}\right)\sin^2\theta + \frac{g_1^2}{2}\sigma_x\left(\frac{1}{\Delta} - \frac{1}{\Omega + \omega_{\rm qb}}\right)\cos\theta\sin\theta + g_2(\sigma_z\cos\theta - \sigma_x\sin\theta) \tag{6}$$

determines the coupling. The interpretation of equations (5) and (6) is that the oscillator frequency depends on the qubit state. This allows dispersive qubit readout by measuring the associated phase shift of the oscillator response upon resonant driving, like in the case of a classical oscillator that is driven by an external force. In particular, assuming that $\cos\theta = 0$ and $g_2 = 0$, equation (5) predicts the frequency shift $\bar{\Omega} = \Omega + \sigma_z g_1^2[1/\Delta - 1/(\Omega + \omega_{\rm qb})]^{-1}$. The last contribution in $\bar{\Omega}$ stems from counter-rotating terms in the qubit–oscillator interaction. These must be accounted for in the case of large detuning Δ, where a rotating-wave approximation produces inaccurate results [34]. Depending on the qubit expectation value $\langle\sigma_z\rangle$, the oscillator is red or blue detuned. Thus, we obtain in this limit the well-known qubit-dependent phase shift corroborated in various experimental realizations [5–8, 22]. There, however, the oscillator frequency was smaller than the qubit splitting, $\Omega \ll \omega_{\rm qb}$. As a consequence, it was only possible to obtain *time-averaged* information about the qubit state.

Now the goal of this paper is generalization of dispersive qubit readout such that *time-resolved* information about the qubit state can be obtained as well. This obviously requires oscillator frequencies and bandwidths larger than the qubit transition frequency, that is, $\Omega \gg \omega_{\rm qb}$. We emphasize that equations (5) and (6) are nevertheless valid as long as the coupling constants are small enough to fulfil condition (3); for details see appendix A and [34]. If the qubit dynamics is much slower than the oscillator, the qubit can be treated within an adiabatic approximation. This means that the qubit dynamics is assumed to be constant during one oscillator period. In turn, the time evolution of the oscillator depends on the instantaneous qubit state. Then

the Schrödinger-picture operators $\sigma_{x,z}$ in equation (6) can be replaced by their time-dependent expectation values, and the operator-valued quantity $\bar{\omega}$ is substituted by

$$\bar{\omega}(t) = \frac{(g_1 \sin\theta)^2}{2}\left(\frac{1}{\Delta} - \frac{1}{\Omega+\omega_{\rm qb}}\right)\langle\sigma_z\rangle_t + \frac{g_1^2}{2}\cos\theta\sin\theta\left(\frac{1}{\Delta} - \frac{1}{\Omega+\omega_{\rm qb}}\right)\langle\sigma_x\rangle_t + g_2\left(\cos\theta\langle\sigma_z\rangle_t - \sin\theta\langle\sigma_x\rangle_t\right). \tag{7}$$

Equation (7) implies that information about the time-dependent qubit state is encoded in the effective oscillator frequency $\bar{\Omega} \equiv \bar{\Omega}(t)$. This gets expressed as a slow parametric modulation in time, like for a parametric oscillator. In detail, the instantaneous qubit state enters via the qubit expectation values $\langle\sigma_{x,z}\rangle_t \equiv {\rm Tr}_{\rm qb}\{\sigma_{x,z}\rho_0(t)\}$, where ${\rm Tr}_{\rm qb}$ denotes the partial trace over the qubit degrees of freedom. The time dependence, indicated by the subscript $\langle\cdots\rangle_t$, stems from the evolution of the total qubit–oscillator state $\rho_0(t)$ under the effective system–bath Hamiltonian (A.15).

As an important intermediate result, the modulation of $\bar{\Omega}$ in time found can be traced back to the qubit dynamics in the absence of the driving. This enables us to measure the qubit's time evolution via the oscillator response to resonant driving.

3. Time-resolved measurement of the qubit dynamics

The qubit–oscillator Hamiltonian in the dispersive picture, equation (4), together with the effective, modulated frequency (5) already indicates that the oscillator detuning may contain information about the qubit dynamics. As in the case of the traditional dispersive readout, we consider the response of the system to an ac field that is resonant with the oscillator. Physically, the situation corresponds to that of a classical mechanical oscillator driven by an external periodic force. Owing to the only weak dissipation, the response is manifest in the phase of the reflected ac driving. In the following, we establish a relation between this phase and a time-dependent qubit expectation value. This relation will form the basis of our measurement protocol.

3.1. Response of the qubit–oscillator compound to resonant driving

In the theory of optical cavities, the response to an external ac excitation is conveniently calculated with the input–output formalism [20, 35]. This formalism has also been applied to quantum circuits [5, 13, 14, 16]. Its cornerstone is the relation

$$\xi_{\rm out}(t) - \xi_{\rm in}(t) = 2\alpha\dot{Q}, \tag{8}$$

formulated in the Heisenberg picture and derived in appendix B. It relates the incoming and the outgoing fluctuations of the transmission line, $\xi_{\rm in/out}(t)$, to the time-derivative of the system-bath coupling operator, which in our case is $Q = a + a^\dagger$. The dimensionless dissipation strength α of the ohmic spectral density quantifies the coupling between the oscillator and the electric environment and, thus, appears as a prefactor. An ac driving corresponds to a coherently excited incoming mode, such that the fluctuations can be separated into quantum fluctuations $\xi_{\rm in}^{\rm qm}(t)$ and a deterministic component $A\cos(\Omega_{\rm ac}t)$. Here, the deterministic part is an ac field in resonance with the bare oscillator, $\Omega_{\rm ac} = \Omega$, such that

$$\xi_{\rm in}(t) = \xi_{\rm in}^{\rm qm}(t) + A\cos(\Omega t), \tag{9}$$

which implies the expectation value $\langle\xi_{\rm in}(t)\rangle = A\cos(\Omega t)$. Then the input–output relation (8) becomes $\xi_{\rm out}(t) = \xi_{\rm in}^{\rm qm}(t) + A\cos(\Omega t) + 2\alpha\dot{Q}$ and thus the corresponding expectation value of the outgoing signal reads

$$\langle\xi_{\rm out}(t)\rangle = A\cos(\Omega t) + 2\alpha\langle\dot{Q}\rangle. \tag{10}$$

It is also convenient to work here in the dispersive picture obtained by the unitary transformation (A.2). While this leaves the environment operators unchanged, the coordinate by which the oscillator couples to the environment changes as $Q \to \bar{Q} = \bar{a} + \bar{a}^\dagger - (\lambda_\Delta - \lambda_\Sigma)\sigma_x + 2\lambda_\Omega\sigma_z$; see equation (A.14). The time derivative $\mathrm{d}\bar{Q}/\mathrm{d}t$ can be obtained from the commutator of $\bar{Q}$ with the Hamiltonian (4) augmented by a term that describes the driving. This yields terms of order Ω and terms with prefactors $\omega_{\rm qb}$ and g_1/Δ. For a fast oscillator, the latter terms can be neglected, and we obtain the equation of motion

$$\frac{\mathrm{d}^2}{\mathrm{d}t^2}\bar{Q} + 2\alpha\bar{\Omega}\frac{\mathrm{d}}{\mathrm{d}t}\bar{Q} + \bar{\Omega}^2\bar{Q} = -2\bar{\Omega}[\xi_{\rm in}^{\rm qm}(t) + A\cos(\Omega t)]. \tag{11}$$

This linear, inhomogeneous equation is readily solved with the help of the Green's function for the dissipative harmonic oscillator. Inserting the resulting $\mathrm{d}\bar{Q}/\mathrm{d}t$ into the input–output relation (10) and neglecting transient terms yields for the expectation value of the outgoing signal the expression

$$\langle\xi_{\rm out}(t)\rangle = A\cos\{\Omega t - \varphi(t)\}. \tag{12}$$

Owing to the weak dissipation, the system energy is almost preserved, such that the amplitudes of the incoming and the outgoing signal are practically the same. The phase difference

$$\varphi(t) = \arctan\left(\frac{-4\alpha\bar{\Omega}\Omega(\bar{\Omega}^2 - \Omega^2)}{(\bar{\Omega}^2 - \Omega^2)^2 - 4\alpha^2\bar{\Omega}^2\Omega^2}\right) \approx \frac{\bar{\Omega}^2 - \Omega^2}{\alpha\Omega\bar{\Omega}} \tag{13}$$

stems from the coupling to the qubit which detunes the oscillator, while the slow time evolution of the qubit renders the phase time-dependent. The approximation is valid if the qubit–oscillator couplings are smaller than the oscillator damping rate, i.e. for $g_1, g_2 \ll \alpha\Omega$. In other words, the first term in the denominator is negligible, since the qubit-induced frequency shift $\bar{\Omega} - \Omega$ is of order $g_{1,2}$. This also ensures $\varphi \ll 1$ and thus $\varphi \approx \tan\varphi$. Next, we insert the effective frequency (5) together with equation (7) and obtain to second order in g_1 and first order in g_2 the phase shift

$$\varphi(t) = \frac{2g_1^2}{\alpha\Omega}\left(\frac{1}{\Delta} - \frac{1}{\Omega + \omega_{\rm qb}}\right)[\sin^2\theta\langle\sigma_z\rangle_t + \cos\theta\sin\theta\langle\sigma_x\rangle_t] + \frac{4g_2}{\alpha\Omega}(\cos\theta\langle\sigma_z\rangle_t - \sin\theta\langle\sigma_x\rangle_t). \tag{14}$$

This central relation forms the basis for our non-invasive qubit measurement via a resonantly driven harmonic oscillator. It identifies a set of qubit observables, which generate the low-frequency system dynamics, as the cause of a small phase shift between the incoming and the outgoing signal. In other words, equation (14) enables one to monitor the qubit dynamics by continuously measuring the phase shift $\varphi(t)$ with suitable experimental techniques.

By evaluating the prefactor for specific setups, we will see below that our measurement scheme is particularly feasible for flux qubits. In this case, the last term of the phase shift (14) dominates, and one measures the qubit variable $\sigma_z\cos\theta - \sigma_x\sin\theta$, i.e. the flux degree of freedom by which the qubit couples to the SQUID; cf the model Hamiltonian (1).

3.2. Static versus dynamical phase shift

The terms entering the phase shift $\varphi(t)$ may be static as well as dynamical. In the first instance, this depends on whether or not the related qubit observables undergo any time evolution. At this point, further insight is obtained by a closer look at the Heisenberg equations of motion for the qubit operators σ_x and σ_z. In the dispersive picture, valid under conditions (3), they are derived from the effective Hamiltonian $\bar{\mathcal{H}}_0$, given by equation (4), and read

$$\dot{\sigma}_x = \frac{\mathrm{i}}{\hbar}[\bar{\mathcal{H}}_0, \sigma_x] = -\omega_{\mathrm{qb}}\sigma_y, \tag{15}$$

$$\dot{\sigma}_z = \frac{\mathrm{i}}{\hbar}[\bar{\mathcal{H}}_0, \sigma_z] = 0. \tag{16}$$

Thus, in the dispersive qubit–oscillator coupling limit (see section 2.2), the observable σ_z is a constant of motion. As a consequence, those contributions to $\varphi(t)$ that depend on $\langle\sigma_z\rangle_t \equiv \langle\sigma_z\rangle_{\mathrm{const}}$ are time-independent. This corresponds again to the established scheme for non-invasive qubit state readout. In contrast, the observable σ_x possesses a non-trivial time dependence generated by $\bar{\mathcal{H}}_0$. Thus, $\langle\sigma_x\rangle_t$ renders the phase shift $\varphi(t)$ dynamical. This, in turn, enables a time-resolved single-run measurement of the unitary qubit evolution by means of the qubit observable σ_x.

According to our measurement relation (14), the dynamical phase signal has the amplitude

$$\varphi^x_{\mathrm{max}} = \frac{2}{\alpha\Omega}\left|g_1^2 \sin\theta\cos\theta\left(\frac{1}{\Delta} - \frac{1}{\Omega+\omega_{\mathrm{qb}}}\right) - 2g_2\sin\theta\right|. \tag{17}$$

Interestingly, φ^x_{max} is reciprocal to the damping strength and the oscillator half-bandwidth $\alpha\Omega$. Thus, a large oscillator frequency together with strong damping leads to reduced angular visibility. On the other hand, the adiabatic treatment of the qubit underlying relation (14) becomes invalid if either Ω or α is too small. Moreover, the input–output relation (10) crucially relies on finite damping. Thus, appropriate choices of Ω and α need to be based upon a compromise between good phase resolution and the validity of our approximations. We go into further details of this issue when discussing the measurement quality in section 4.2.

It is important to note that the amplitude φ^x_{max} possesses contributions from both the linear and the quadratic qubit–oscillator interaction of Hamiltonian (1). The first term on the rhs of equation (17) stems from the linear interaction characterized by the coupling coefficient g_1. Like the effective Hamiltonian (A.13), this contribution is of second order in the dispersive parameter g_1/Δ. Due to the minus sign in round brackets, it is additionally minimized, given that $\Delta/(\Omega+\omega_{\mathrm{qb}}) \approx 1$ for large detuning Δ. Thus, for a Cooper-pair box or a flux qubit coupled to a high-frequency transmission line resonator, where the qubit–oscillator coupling merely depends on the circuit characteristics and is therefore purely linear, i.e. $g_2 = 0$, the maximum amplitude φ^x_{max} drops below any useful level.

On the contrary, a finite quadratic qubit–oscillator interaction $g_2 > 0$ ensures a noticeable phase signal, independent of the detuning Δ, and even if $g_2 \ll g_1$. Formally, this feature arises from Hamiltonian (1), where the quadratic coupling term already generates a frequency shift in zeroth order perturbation theory. If the qubit–oscillator interaction is transverse, that is, $\epsilon = 0$, the phase resolution is maximized, whereas it vanishes for purely longitudinal coupling, i.e. for $\delta = 0$. Hence, the presence of a nonlinear qubit–oscillator interaction, as provided by a nonlinear SQUID Josephson inductance, turns out to be a crucial ingredient.

4. Measurement quality

The central measurement relations (14) and (17) remain to be corroborated, via comparing them with the phase shift obtained by simulating the actual measurement process. In doing so, we restrict ourselves to the fundamental example of coherent qubit oscillations. For the numerical treatment of the qubit–oscillator state, we employ the quantum master equation (C.1) derived from the full dissipative qubit–oscillator–bath Hamiltonian (2). For a realistic evaluation, we use parameters similar to those of the experiment reported in [18, 19]. Furthermore, we employ $N = 10$ oscillator states, which turns out to be sufficient to reach numerical convergence.

4.1. Time-resolved measurement of unitary qubit evolution

If the qubit is only weakly coupled to the oscillator, and if the latter is driven only weakly, the qubit's time evolution is rather coherent (see section 4.3 on qubit decoherence). For this scenario, figure 2(a) depicts the time-dependent phase $\varphi(t)$ computed with the measurement relation (14), while the inset confirms its proportionality to the qubit expectation value $\langle\sigma_x\rangle_t$. For comparison, we wish to recover this phase information directly by analysing the outgoing signal $\langle\xi_{\rm out}(t)\rangle$, as given by equation (10). In an experiment, this can be achieved by lock-in techniques, which we mimic in the following way [36]. First, we focus on the associated spectrum $\langle\xi_{\rm out}(\omega)\rangle$ depicted in figure 2(b). It reflects the qubit dynamics in terms of two sidebands around the central peak related to the oscillator frequency, here chosen as $\Omega = 10\,\omega_{\rm qb}$. The dissipative influence of the environment, modelled by a transmission line (see figure 1), is reflected in a broadening of this peak. The corresponding oscillator bandwidth is given as $2\alpha\Omega$, where α denotes the dimensionless damping strength; see appendix C. Here, we recall that the oscillator is driven resonantly by the external driving signal $A\cos(\Omega_{\rm ac}t)$, that is, $\Omega = \Omega_{\rm ac}$. In the time domain, the sidebands correspond to the phase-shifted signal $\langle\xi_{\rm out}(t)\rangle = A\cos(\Omega t - \varphi_{\rm exp}(t))$ with a slowly time-dependent phase $\varphi_{\rm exp}(t)$. In order to obtain this phase $\varphi_{\rm exp}(t)$, we select the spectral data from a frequency window of size $2\Delta\Omega$ centred at the oscillator frequency Ω, which means that $\langle\xi_{\rm out}(\omega)\rangle$ is multiplied by a Gaussian window function $\exp(-(\omega-\Omega)^2/\Delta\Omega^2)$. We choose for the window size the resonator bandwidth, $\Delta\Omega = \alpha\Omega$, which turns out to suppress disturbing contributions from the low-frequency qubit dynamics. Finally, we centre the clipped spectrum at zero frequency and perform an inverse Fourier transform to the time domain. If the phase shift $\varphi_{\rm exp}$ is constant, one could use a much smaller measurement bandwidth. Then the outcome of the measurement procedure would correspond to homodyne detection [35] of a quadrature defined by the phase shift and yield a value $\propto \cos\varphi_{\rm exp}$.

Figure 2(a) reveals the good agreement of the resulting $\varphi_{\rm exp}(t)$ with the prediction of our measurement relation, $\varphi(t) \propto \langle\sigma_x\rangle_t$, at angular resolutions of 1–2°. Good agreement is already obtained for an oscillator frequency $\Omega = 10\,\omega_{\rm qb}$, which obviously represents a good compromise between the validity of the adiabatic approximation (see section 2.2) and a sufficiently strong signal. There is even some room for obtaining a stronger phase signal since the dissipation strength α still can be reduced without violating the validity range of our theory as long as $\omega_{\rm qb} \lesssim \Delta\Omega$.

Setting either g_1 or g_2 to zero (not shown) reveals that the nonlinear coupling g_2 is responsible for the good agreement of the phase shifts in figure 2(a). Thus, the whole protocol is mainly applicable to flux qubits coupled to SQUIDs. For charge qubits, by contrast, the typical values of g_2 are too small. Furthermore, we have verified that the visible constant delay between

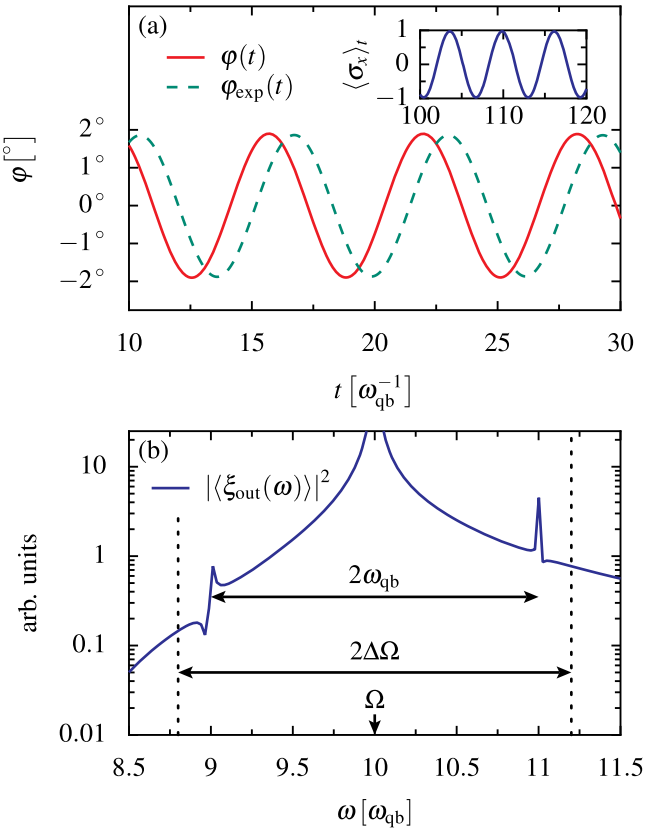

Figure 2. Time-resolved measurement of coherent qubit oscillations at the degeneracy point $\epsilon = 0$. The full qubit–oscillator state was simulated with the quantum master equation (C.1) with $N = 10$ oscillator states and the parameters $\Omega = \Omega_{\rm ac} = 10\,\omega_{\rm qb}$, $g_1 = 0.1\,\omega_{\rm qb}$, $g_2 = 0.01\,\omega_{\rm qb}$, $A = 1.0\,\omega_{\rm qb}$. The dimensionless oscillator dissipation strength is $\alpha = 0.12$. The resonator bandwidth is given by $2\alpha\Omega = 2.4\omega_{\rm qb}$. (a) Lock-in amplified phase $\varphi_{\rm exp}(t)$ (dashed green lines), compared to the estimated phase $\varphi(t)$ (solid red line) of the outgoing signal $\langle\xi_{\rm out}(t)\rangle$. Here, $\varphi(t) \propto \langle\sigma_x\rangle_t$ (cf equation (14)), which is corroborated by the inset showing that $\langle\sigma_x\rangle_t$ performs oscillations with (angular) frequency $\omega_{\rm qb}$. (b) Power spectrum $\langle\xi_{\rm out}(\omega)\rangle$ for the resonantly driven oscillator (blue solid line). The sidebands stemming from the qubit dynamics are visible at frequencies $\Omega \pm \omega_{\rm qb}$. In order to extract the phase information, we apply a Gaussian window function with respect to the frequency window of half-width $\Delta\Omega = 1.2\omega_{\rm qb}$, which turns out to be the optimal value for the measurement bandwidth.

both phases $\varphi(t)$ and $\varphi_{\rm exp}(t)$ does not depend on the selected parameters, while its detailed origin remains unexplained.

4.2. Measurement characterization: fidelity and backaction

The validity of relation (14) for the phase $\varphi(t)$ is naturally limited to specific parameter ranges due to the various underlying approximations made. The main crucial assumptions to justify the

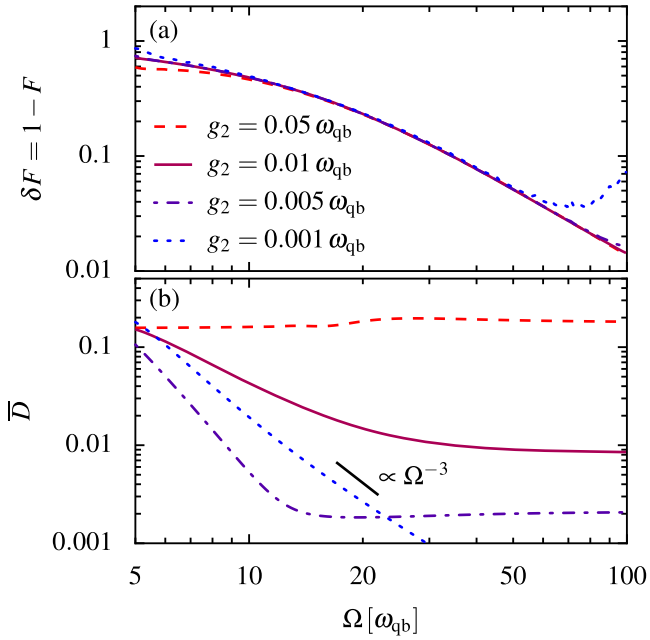

Figure 3. (a) Fidelity defect $\delta F = 1 - F$ for the phases $\varphi(t)$ and $\varphi_{exp}(t)$ and (b) time-averaged trace distance $\bar{D}$ between the density operators of a qubit with finite coupling to the oscillator and a reference qubit without oscillator. Both quantities are depicted for various coupling strengths g_2 in dependence of the oscillator frequency Ω. All other parameters are the same as in figure 2.

adiabatic treatment of the qubit are a large qubit–oscillator detuning $\Delta/\Omega \simeq 1$ and weak mutual interaction, $g_2 \ll g_1 \ll \Delta$. Furthermore, the oscillator damping α is assumed to stay within the limits $g_{1,2}/\Omega \ll \alpha \ll 1$.

In an experiment, the oscillator frequency and the coupling strength are finite, however. Consequently, the actual phase $\varphi_{exp}(t)$, which we extract numerically and which can be measured by lock-in amplification, generally differs from the predicted phase $\varphi(t)$. Thus, the mutual agreement of both phases needs to be tested quantitatively for realistic scenarios. To this end, we employ the measurement fidelity F with the scaled overlap defined as

$$F = (\varphi, \varphi_{exp}) \equiv \left[\int \mathrm{d}t\, \varphi^2(t) \int \mathrm{d}t\, \varphi_{exp}^2(t)\right]^{-1/2} \left|\int \mathrm{d}t\, \varphi(t)\varphi_{exp}(t)\right|. \tag{18}$$

The ideal value of $F = 1$ is assumed if $\varphi(t) \propto \varphi_{exp}(t)$.

In figure 3(a) we depict the fidelity defect $\delta F = 1 - F$ between $\varphi_{exp}(t)$ and $\varphi(t)$ as a function of the oscillator frequency $\Omega = \Omega_{ac}$ for different quadratic coupling coefficients g_2. As expected, the overall fidelity is rather insufficient for small oscillator frequency $\Omega < 10\omega_{qb}$, for which the adiabatic approximation of section 2.2 is not valid and, moreover, if the oscillator bandwidth is too small to resolve the qubit dynamics, i.e. if $\omega_{qb} < \alpha\Omega$. When we increase Ω, the fidelity defect δF drops to values of 0.05–0.5, independently of the parameter g_2. Taking into account that the fidelity is arbitrarily lowered by the constant delay between $\varphi(t)$ and $\varphi_{exp}(t)$ visible in figure 2, this still corroborates that $\Omega = 10\omega_{qb}$ is a good choice. In the limit of large oscillator frequencies, we again observe an increase in the fidelity defect, which occurs sooner the smaller g_2 is. This latter effect, which is only visible for the smallest value of g_2 in figure 3(a),

is directly explained by a reduced maximum angular visibility of the phase $\varphi(t) \propto g_2/\Omega$. Thus, figure 3(a) provides a pertinent indication for the validity frame of our central relation (14).

Moreover, it is necessary to take into account the backaction upon the qubit that stems from the nonlinear qubit–oscillator interaction. An appropriate measure for how much the qubit dynamics is perturbed by the oscillator is given by the time average $\bar{D}$ of the trace distance $D(t) = \frac{1}{2}\mathrm{Tr}|\rho_{\mathrm{qb}}(t) - \rho_{\mathrm{qb},0}(t)|$ between the qubit dynamics with and without the coupling to the driven oscillator. To be specific, we compare the qubit state $\rho_{\mathrm{qb}}(t)$ evolving under the full system–bath Hamiltonian (2) to an unperturbed reference state $\rho_{\mathrm{qb},0}(t)$ that evolves unitarily under the bare qubit Hamiltonian $\mathcal{H}_{\mathrm{qb}} = (\hbar\omega_{\mathrm{qb}}/2)\sigma_z$. Thus, the trace distance essentially quantifies the invasiveness of the measurement based upon the second-order qubit–oscillator interaction. In the absence of perturbations to the qubit, $\bar{D}$ vanishes by definition, while $\bar{D} = 1$ if the density operator of the measured qubit is completely unrelated to that of the reference.

Figure 3(b) shows that the predicted phase $\varphi(t)$ faithfully describes the unperturbed qubit dynamics as long as the coefficient g_2 stays sufficiently small. A reliable operating range appears to be $g_2/\omega_{\mathrm{qb}} \lesssim 0.01$. For $\Omega = 10\,\omega_{\mathrm{qb}}$, this is consistent with our above reasoning regarding the fidelity. For even weaker quadratic interactions, we first find $\bar{D} \propto \Omega^{-3}$, which implies that the dispersive first-order coupling in terms of g_1 governs the qubit–oscillator interaction when Ω is small. This cubic dependence is due to relation (14) and to the fact that the first-order perturbation acting on the qubit has an inverse quadratic dependence on the detuning $\Delta \propto \Omega$. Beyond a critical detuning, which individually depends on g_2, the quadratic interaction prevails again, as is reflected by the saturation of $\bar{D}$ with increasing oscillator frequency Ω. For $g_2/\omega_{\mathrm{qb}} \gtrsim 0.05$, the effect of the linear coupling withers. Thus, at $g_2 = 0.01\omega_{\mathrm{qb}}$, the value of g_1 is rather irrelevant for our measurement protocol.

4.3. Signal-to-noise ratio

Generally, a signal can be resolved only if its spectral density exceeds the level of background noise at the measurement frequency. In the present scheme, the desired information is contained in the sidepeaks of the spectrum at $\Omega \pm \omega_{\mathrm{qb}}$; see figure 2(b). For the corresponding phase-modulated oscillation $A\cos(\Omega t - \varphi_{\max}\sin(\omega_{\mathrm{qb}}t))$, these sidepeaks correspond in the time domain to the oscillation $A\varphi_{\max}\sin(\omega_{\mathrm{qb}}t)$. If the signal is integrated for a time t, its spectral weight becomes $(A\varphi_{\max})^2 t$. The phase amplitude $\varphi_{\max}$ is given by equation (17), but for the present purpose, it is sufficient to consider the dominating contribution, which is the one proportional to g_2. Thus, here $\varphi_{\max} = 4g_2/\alpha\Omega$, while we restrict ourselves to the case $\theta = \pi/2$.

Since the measured signal corresponds to the state of a highly excited environmental mode, the relevant noise level is determined by the fluctuations of the effective bath coordinate ξ. If the temperature is sufficiently low, such that thermal excitations do not play any role, its spectral density equals the bath spectral density: $S_{\xi\xi}(\omega) = J(\omega) = \alpha\omega$. Thus, the signal is at least as big as the noise background if $J(\Omega) \leqslant (A\varphi_{\max})^2 t$. In other words, the time t during which the output is recorded must fulfil

$$t \geqslant \frac{4J(\Omega)}{(A\varphi_{\max})^2} = \frac{(\alpha\Omega)^3}{(2g_2A)^2} \equiv t_{\mathrm{meas}}. \tag{19}$$

For the parameters used in figure 2, $t_{\mathrm{meas}} \approx 4 \times 10^3/\omega_{\mathrm{qb}}$.

Since the measurement is carried out via a coupling to external degrees of freedom, the qubit experiences unavoidable decoherence, which means that coherent qubit oscillations

fade away with a decoherence rate γ_ϕ. The time during which meaningful information can be obtained is therefore limited by the inequality $t \leqslant 1/\gamma_\phi$. This condition together with condition (19) can be fulfilled only if $\gamma_\phi t_{\rm meas} \geqslant 1$.

The decoherence rate can be estimated upon noticing that our qubit Hamiltonian represents a generalized spin-boson model [24–26] with the bath coupling $\frac{1}{2}\sigma_x\eta$, where $\eta = 2g_2Q^2$ is the effective bath coordinate. For weak dissipation, γ_ϕ is given by the auto-correlation function of the latter evaluated at the qubit splitting, i.e. $\gamma_\phi = C_{\eta\eta}(\omega_{\rm qb})$ [37]. This still holds true in the presence of ac driving provided that the driving-induced renormalization of the qubit splitting is negligible [38]. We separate the qubit coordinate into the responses to the driving and to the incoming fluctuations, $Q = \langle Q\rangle + \delta Q$; cf equation (9). Then we proceed along the lines of [39]; the relevant terms are those of second order in δQ, such that $C_{\eta\eta}(t) \approx 4g_2^2(A/\alpha\Omega)^2\cos(\Omega t)\langle\delta Q(t)\delta Q(0)\rangle$. By Fourier transformation, we obtain to lowest order in $\omega_{\rm qb}/\Omega$ the decoherence rate

$$\gamma_\phi = \frac{(2g_2A)^2}{(\alpha\Omega)^3}, \tag{20}$$

which is the inverse of the required measurement time $t_{\rm meas}$. A comparison with the numerically computed decay of the qubit coherence (not shown) confirms this value. The obtained relation $\gamma_\phi t_{\rm meas} = 1$ marks the quantum limit of a measurement [39] and allows one to marginally fulfil both conditions on the measurement time t.

4.4. A possible experimental implementation

Specific parameters can be obtained for the setup of [19] for which the qubit-oscillator coupling parameters are determined by the flux bias current $I_{\rm b}$ and read

$$g_1 = -\frac{MI_{\rm p}}{4\hbar I_{\rm C}}\frac{\sin(\varphi/2)}{\cos^2(\varphi/2)}\sqrt{\frac{\hbar\Omega}{2L_{\rm J}}}I_{\rm b}, \tag{21}$$

$$g_2 = -\frac{MI_{\rm p}}{16L_{\rm J}I_{\rm C}}\frac{\sin(\varphi/2)}{\cos^2(\varphi/2)}\Omega. \tag{22}$$

Here, M denotes the mutual SQUID–qubit inductance, $I_{\rm p}$ is the qubit persistent-current, $I_{\rm C}$ the critical current of the SQUID Josephson junctions, and $L_{\rm J} = \phi_0[4\pi I_{\rm C}\cos(\pi\phi_{\rm SQ}/\phi_0)]^{-1}$ the SQUID Josephson inductance. The flux $\phi_{\rm SQ}$ that penetrates the SQUID loop corresponds to the phase $\varphi = 2\pi\phi_{\rm SQ}/\phi_0$, with $\phi_0 = h/2e$ being the flux quantum. For small bias currents $I_{\rm b}$ while neglecting the inductance of the wire that leads to the shunting capacitance C, the oscillator frequency is approximately given by the SQUID plasma frequency $\Omega = |L_{\rm J}C|^{-1/2}$.

For a typical qubit transition frequency of $\omega_{\rm qb}/2\pi = 5\,$GHz, resolving the qubit dynamics requires an oscillator frequency of $\Omega/2\pi = 10\omega_{\rm qb}/2\pi = 50\,$GHz. The necessary lock-in measurements at a carrier frequency $\Omega/2\pi = 50\,$GHz are particularly challenging at low temperatures, but are feasible [40]. They require rather expensive amplifying technology such as cryogenic amplifiers developed by Low Noise Factory (Sweden). Recently suitable devices developed can be operated at up to 36 GHz and possess reasonably low noise temperatures.

Alternatively, a Josephson parametric amplifier [41, 42] enables the detection of oscillator frequencies as high as $\Omega/2\pi = 20$–$25\,$GHz. Thus, as a compromise, we restrict ourselves to an oscillator frequency of $\Omega/2\pi = 24\,$GHz, which is suitable for detecting the dynamics of

a qubit with $\omega_{\rm qb}/2\pi = 2.5\,$GHz, a value still large enough to avoid thermal excitations at working temperatures of 20 mK. The above value for Ω can be realized using the parameters $I_{\rm C} = 4.25\,\mu$A, $\varphi = 2.3\pi$ and $C = 1\,$pF, which are similar to those of [18, 19]. Along with $M = 17.5\,$pH, $I_{\rm p} = 300\,$nA and $I_{\rm b} = 0.4\,\mu$A, we obtain the qubit–oscillator coupling coefficients $g_1/2\pi = 45\,$MHz and $g_2 = 24\,$MHz. Thus, the relevant dimensionless coupling assumes the value $g_2/\omega_{\rm qb} \simeq 0.01$ used in our numerical studies. An adequate oscillator half-bandwidth is $\Delta\Omega = 2.9\,$GHz, which implies a low external quality factor of $Q \simeq 4$–5.

Our two-state model for the qubit does not consider possible excitations to non-qubit states caused by the coupling to the oscillator. Nevertheless, our modelling is appropriate, because such leakage has far less relevance than for a Cooper-pair box, owing to the fact that the higher states couple only weakly to the SQUID [43]. Apart from this, it is possible to design or tune the oscillator such that its frequency is far from any qubit resonance. The required oscillator frequency of the order of 10 GHz is still significantly smaller than the gap energy of aluminium, such that quasi-particle excitation should not play a major role. This issue is even less critical for niobium.

5. Conclusions

We have generalized dispersive qubit readout to the time-resolved observation of the qubit dynamics. Concerning the setup, the main difference to dispersive readout is that in the present proposal, the oscillator frequency needs to exceed the qubit splitting by roughly one order of magnitude, and the oscillator bandwidth should be at least twice the qubit frequency. Also, here the oscillator frequency becomes dynamically red or blue detuned, depending on the state of the qubit. When driving the SQUID oscillator at its bare frequency Ω, this detuning turns into a phase shift visible in the reflected signal via lock-in techniques. For such a qubit measurement using the oscillator phase, the oscillator frequency represents the sampling rate, which explains the need for high frequencies.

The constituting measurement relation has been derived from the input–output formalism under time-scale separation of the bare qubit dynamics from the oscillator. A numerical solution of the Bloch–Redfield master equation for the full qubit–oscillator dynamics also allowed us to compute the phase of the reflected signal directly. Its good agreement with the phase predicted by our measurement relation confirms the validity of the latter even when the oscillator frequency is only moderately large. Thus, there is no need to drive the qubit with extremely high frequencies, which would be quite challenging in an experiment. The agreement found is also reflected by the measurement fidelity, which for moderate frequencies is already rather good. Furthermore, the numerical analysis has demonstrated that the external ac driving does not significantly modify the qubit dynamics, which means that the backaction of the measurement process is weak. However, it must be emphasized that the whole scheme relies on the coupling of the qubit via the oscillator to a dissipative environment, which already causes qubit decoherence when the external driving is not active. In the limit of far qubit–oscillator detuning, this qubit decoherence is drastically reduced, however.

An evaluation of the measurement relation for parameters of recent experiments with flux qubits predicts phase shifts up to 2°, which can be measured. Moreover, it reveals that the signal mainly stems from the coupling of the qubit to the square of the oscillator coordinate. The linear coupling to the coordinate, by contrast, leads to a rather small phase shift. This means that the measured quantity is essentially the qubit's flux degree of freedom. Likewise, the linear

coupling of a superconducting charge qubit to a waveguide resonator is also too weak. Since for this system the nonlinear coupling practically vanishes, the measured signal remains tiny. In conclusion, using current technology our measurement protocol should be most feasible with flux qubits coupled to SQUIDs that possess a significant nonlinear Josephson inductance. All in all, our proposal may initiate further progress on the way towards single-shot experiments that demonstrate quantum coherence in solid-state devices.

Acknowledgments

We thank Klaus Mølmer, Alexander Baust, Frank Deppe, and Max Häberlein for fruitful discussions. This work was supported by the German Research Foundation (DFG) through the Collaborative Research Centre SFB 631 and through the German Excellence Initiative via the 'Nanosystems Initiative Munich (NIM)'. We also acknowledge support from the Spanish Ministry of Science and Innovation (MICINN) through grant numbers MAT2008/02626 (SK), FIS2008-01240 and FIS2009-13364-C02-0 (DZ).

Appendix A. System–bath Hamiltonian in the dispersive coupling limit

In the limit of large oscillator–qubit detuning, the coupling coefficients automatically fulfil the conditions

$$g_1,\ g_2 \ll \Delta, \quad \Delta = \Omega - \omega_{\rm qb}, \tag{A.1}$$

which mark the dispersive coupling regime. Following [32, 33], the effective Hamiltonian $\mathcal{H}_{0,\rm disp} = \mathcal{U}^\dagger \mathcal{H}_0 \mathcal{U}$ is then obtained from the full system Hamiltonian (1) by the unitary transformation

$$\mathcal{U} = \exp(\lambda_\Delta \mathcal{D} + \lambda_\Sigma \mathcal{S} + \lambda_\Omega \mathcal{W}), \tag{A.2}$$

where

$$\mathcal{D} = \sigma^- a^\dagger - \sigma^+ a, \tag{A.3}$$

$$\mathcal{S} = \sigma^- a - \sigma^+ a^\dagger, \tag{A.4}$$

$$\mathcal{W} = \sigma_z (a - a^\dagger). \tag{A.5}$$

Defining $\Sigma = \omega_{\rm qb} + \Omega$, the necessarily small and dimensionless dispersive parameters

$$\lambda_\Delta = -\frac{g_1 \sin\theta}{\Delta}, \tag{A.6}$$

$$\lambda_\Sigma = \frac{g_1 \sin\theta}{\Sigma}, \tag{A.7}$$

$$\lambda_\Omega = -\frac{g_1 \cos\theta}{\Omega} \tag{A.8}$$

emerge. Expanding the transformed Hamiltonian in powers of $\lambda_{\Delta,\Sigma,\Omega}$, we obtain to second dispersive order the effective Hamiltonian

$$\bar{\mathcal{H}}_0 = \hbar\Omega \left(a^\dagger a + \frac{1}{2}\right) + \frac{\hbar\omega_{\rm qb}}{2}\sigma_z + \frac{\hbar}{2}(\Delta\lambda_\Delta^2 - \Sigma\lambda_\Sigma^2)\sigma_z (a + a^\dagger)^2 + \frac{\hbar\Omega}{2}\lambda_\Omega\,(\lambda_\Delta + \lambda_\Sigma)\,\sigma_x (a + a^\dagger)^2$$
$$- \frac{{\rm i}\omega_{\rm qb}}{2}\lambda_\Omega(\lambda_\Delta + \lambda_\Sigma)\sigma_y (a^2 - (a^\dagger)^2) + g_2(\cos\theta\sigma_z - \sin\theta\sigma_x)(a + a^\dagger)^2. \tag{A.9}$$

The third and fourth terms of this Hamiltonian constitute corrections to the curvature of the oscillator potential, i.e. the prefactor of $(a+a^\dagger)^2$. They stem from the linear qubit–oscillator interaction and thus enter only in the second dispersive order. Since we consider a high-frequency oscillator, the detuning is always positive, $\Delta > 0$, such that the dispersive parameters λ_Δ and λ_Σ are of opposite sign. Thus, in the case of far dispersive detuning $\Omega \gg \omega_{\rm qb}$, these terms become rather small. In spite of this, we keep them for later use. In contrast, we can safely neglect the fifth term that is not of the shape $(a+a^\dagger)^2$ and whose coefficient is small as compared to the other terms.

The last term of equation (A.9), stemming from the second-order interaction between qubit and oscillator, plays a particular role. Since it is already of the second order in the oscillator coordinate $a+a^\dagger$ and its coefficient g_2 is correspondingly small, $g_2 \ll g_1$, it is not affected by the transform (A.2). As a consequence, this term remains independent of the qubit–oscillator detuning Δ, for which reason its contribution to the $(a+a^\dagger)^2$-terms is finite.

For further convenience, we introduce transformed creation and annihilation operators that describe the oscillator–qubit system in the adiabatic limit $\Omega \gg \omega$,

$$\bar{a} = \frac{1}{2}\sqrt{\frac{\bar{\Omega}}{\Omega}}(a+a^\dagger) + \frac{1}{2}\sqrt{\frac{\Omega}{\bar{\Omega}}}(a-a^\dagger), \tag{A.10}$$

and $\bar{a}^\dagger$ accordingly, such that $[\bar{a}, \bar{a}^\dagger] = 1$. The effective oscillator frequency

$$\bar{\Omega} = \Omega\sqrt{1+\frac{4\bar{\omega}}{\Omega}} \tag{A.11}$$

accounts for all quadratic corrections to the oscillator potential in the effective Hamiltonian (A.9) in terms of the effective operator-valued coupling frequency

$$\bar{\omega} = \tfrac{1}{2}(\Delta\lambda_\Delta^2 - \Sigma\lambda_\Sigma^2)\sigma_z + \tfrac{1}{2}\Omega\lambda_\Omega(\lambda_\Delta+\lambda_\Sigma)\sigma_x + g_2(\cos\theta\sigma_z - \sin\theta\sigma_x). \tag{A.12}$$

Thus, the effective Hamiltonian can be rewritten as

$$\bar{\mathcal{H}}_0 = \hbar\bar{\Omega}(\bar{a}^\dagger\bar{a} + \tfrac{1}{2}) + \tfrac{1}{2}\hbar\omega_{\rm qb}\sigma_z. \tag{A.13}$$

Put differently, the qubit–oscillator coupling has been shifted to the effective operator-valued oscillator frequency $\bar{\Omega}$, which depends on the qubit state.

In order to move fully to the dispersive picture, we also have to transform the system operator $Q = a + a^\dagger$ by which the oscillator couples to the environment. Transformation with the operator (A.2) yields in first dispersive order the position operator

$$\bar{Q} = \mathcal{U}^\dagger Q \mathcal{U} = (\bar{a}+\bar{a}^\dagger) - (\lambda_\Delta - \lambda_\Sigma)\sigma_x + 2\lambda_\Omega\sigma_z, \tag{A.14}$$

where we have assumed that $\Omega \approx \bar{\Omega}$. The full system–bath Hamiltonian in the dispersive picture finally reads as

$$\bar{\mathcal{H}} = \bar{\mathcal{H}}_0 + \hbar\bar{Q}\sum_n c_n(b_n + b_n^\dagger) + \sum_n \hbar\omega_n(b_n^\dagger b_n + \tfrac{1}{2}). \tag{A.15}$$

Appendix B. Input–output formalism

In order to compute the response of the oscillator to the external driving, we employ the input-output formalism [20], which is most conveniently obtained from the quantum Langevin

equation of the central system [44–47]. We derive it from the system–bath Hamiltonian (2) via the Heisenberg equation of motion for the bath oscillator coordinates $q_n = b_n + b_n^\dagger$,

$$\ddot{q}_n + \omega_n^2 q_n = 2c_n\omega_n Q. \tag{B.1}$$

Here, the oscillator coordinate $Q = a + a^\dagger$ enters as inhomogeneity. The formal solution of equation (B.1) for initial time t_0 is

$$q_n(t) = q_n(t_0)\cos\{\omega_n(t-t_0)\} + \frac{p_n(t_0)}{\omega_n}\sin\{\omega_n(t-t_0)\} + 2c_n\int_{t_0}^{t} \mathrm{d}t'\ \sin\{\omega_n(t-t')\}Q(t'), \tag{B.2}$$

with $p_n(t_0) = \dot{q}_n(t_0)$. Inserting this solution into the Heisenberg equation of motion for Q yields

$$\begin{aligned}\ddot{Q} = &-\Omega^2 Q - 4\Omega\sum_n c_n^2\int_{t_0}^{t}\mathrm{d}t'\sin\{\omega_n(t-t')\}Q(t') \\ &- 2\Omega\sum_n c_n\left(q_n(t_0)\cos\{\omega_n(t-t_0)\} + \frac{p_n(t_0)}{\omega_n}\sin\{\omega_n(t-t_0)\}\right).\end{aligned} \tag{B.3}$$

For the sake of a compact notation, we define the operator for the incoming fluctuations,

$$\xi_{\mathrm{in}}^{\mathrm{qm}}(t) = \sum_n c_n\left(q_n(t_0)\cos\{\omega_n(t-t_0)\} + \frac{p_n(t_0)}{\omega_n}\sin\{\omega_n(t-t_0)\}\right), \tag{B.4}$$

which only depends on the environmental operators at initial time and thus is independent of the central quantum system.

We replace the sum $\sum_n |c_n|^2$ by an integral over the spectral density $J(\omega)/\pi$, which for the ohmic $J(\omega) = \alpha\omega$ becomes the derivative of the delta function $\delta(t-t')$, such that the time integral can be evaluated. In doing so, we arrive at the quantum Langevin equation

$$\ddot{Q} + 2\alpha\Omega\dot{Q} + \Omega^2 Q = -2\Omega\xi_{\mathrm{in}}^{\mathrm{qm}}(t), \tag{B.5}$$

where we have discarded an initial slip term and a constant potential renormalization, which are both not relevant in the present context and beyond transient behaviour. Note that dissipation enters via a friction term, while the incoming fluctuations act as a stochastic driving force.

The quantum Langevin equation (B.5) can also be expressed in terms of the outgoing fluctuations by solving the equations of motion (B.1) for q_n with boundary condition at a later time $t_1 > t$, i.e. by backward propagation. Then one obtains

$$q_n(t) = q_n(t_1)\cos\{\omega_n(t-t_1)\} + \frac{p_n(t_1)}{\omega_n}\sin\{\omega_n(t-t_1)\} + 2c_n\int_{t}^{t_1}\mathrm{d}t'\ \sin\{\omega_n(t-t')\}Q(t'). \tag{B.6}$$

The corresponding environment operators define the outgoing fluctuations

$$\xi_{\mathrm{out}}^{\mathrm{qm}}(t) = \sum_n c_n\left(q_n(t_1)\cos\{\omega_n(t-t_1)\} + \frac{p_n(t_1)}{\omega_n}\sin\{\omega_n(t-t_1)\}\right). \tag{B.7}$$

In contrast to $\xi_{\mathrm{in}}^{\mathrm{qm}}(t)$, this noise operator depends on the time evolution of the system at earlier times $t < t_1$. The resulting Langevin equation for the oscillator coordinate Q,

$$\ddot{Q} - 2\alpha\Omega\dot{Q} + \Omega^2 Q = -2\Omega\xi_{\mathrm{out}}^{\mathrm{qm}}(t), \tag{B.8}$$

is characterised by negative damping and the outgoing noise. The difference of both Langevin equations links the noise terms via twice the dissipative term by means of the input-output relation, which in the stationary limit $t_0 \to -\infty$ and $t_1 \to \infty$ reads [20]

$$\xi_{\mathrm{out}}^{\mathrm{qm}}(t) - \xi_{\mathrm{in}}^{\mathrm{qm}}(t) = 2\alpha\dot{Q}. \tag{B.9}$$

Even though we have written this relation for a harmonic oscillator, the derivation does not rely on particular properties of this system. Thus, equation (B.9) is valid as well for nonlinear quantum systems coupled to an environment.

If a bath mode is coherently excited by an external driving field, the incoming fluctuations are augmented by a deterministic contribution, $\xi_{\rm in}^{\rm qm} \to \xi_{\rm in}^{\rm qm} + x_{\rm drive}(t)$. Then the input-output relation allows one to compute both the averaged outgoing signal as well as its fluctuations and noise spectra.

Appendix C. Bloch–Redfield master equation

The numerical data presented in section 4 have been computed with a quantum master equation of the Bloch–Redfield type [48],

$$\dot{\rho}_0(t) = -\frac{\mathrm{i}}{\hbar}[\mathcal{H}_0, \rho_0(t)] - [Q, [\hat{Q}, \rho_0(t)]] + \mathrm{i}\alpha[Q, \{\dot{Q}, \rho_0(t)\}], \tag{C.1}$$

where

$$\hat{Q} = \frac{\alpha}{\pi}\int_0^\infty \mathrm{d}\tau \int_0^\infty \mathrm{d}\omega\, \omega \coth\!\left(\frac{\hbar\omega}{2k_{\rm B}T}\right)\cos(\omega\tau)\tilde{Q}(-\tau). \tag{C.2}$$

It describes the time evolution of the reduced density operator $\rho_0(t)$ of the qubit plus the oscillator. The dissipative terms have been derived under the assumption that the bath couples weakly to a system operator Q with a vanishing equilibrium expectation value. The environment is in a thermal state at temperature T, and the system–bath interaction possesses the ohmic spectral density $J(\omega) = \alpha\omega$ with the dimensionless damping strength α. Furthermore, $\tilde{X}(t) = \mathcal{U}_0^\dagger(t, t_0)X\mathcal{U}_0(t, t_0)$ refers to the time evolution of the system operator X in an interaction picture described by the propagator $\mathcal{U}_0(t, t_0) = \exp\{\mathrm{i}\mathcal{H}_0(t - t_0)/\hbar\}$, and $\dot{Q}$ is a shorthand notation for the Heisenberg time derivative $\mathrm{i}[\mathcal{H}_0, Q]/\hbar$ of the system–bath coupling operator Q.

References

[1] Zurek W H 2003 *Rev. Mod. Phys.* **75** 715
[2] Nakamura Y, Pashkin Y A and Tsai J S 1999 *Nature* **398** 786
[3] Leek P J, Fink J M, Blais A, Bianchetti R, Göppl M, Gambetta J M, Schuster D I, Frunzio L, Schoelkopf R J and Wallraff A 2007 *Science* **318** 1889
[4] Ansmann M *et al* 2009 *Nature* **461** 504
[5] Sillanpää M A, Lehtinen T, Paila A, Makhlin Y, Roschier L and Hakonen P J 2005 *Phys. Rev. Lett.* **95** 206806
[6] Lupascu A, Driessen E F C, Roschier L, Harmans C J P M and Mooij J E 2006 *Phys. Rev. Lett.* **96** 127003
[7] S A L, Saito, Picot T, de Groot P C, Harmans C J P M and Mooij J E 2007 *Nat. Phys.* **3** 119
[8] Schuster D I *et al* 2007 *Nature* **445** 515
[9] Ashhab S, You J Q and Nori F 2009 *Phys. Rev.* A **79** 032317
[10] Ashhab S, You J Q and Nori F 2009 *New J. Phys.* **11** 083017
[11] Chiorescu I, Bertet P, Semba K, Nakamura Y, Harmans C J P M and Mooij J E 2004 *Nature* **431** 159
[12] Wallraff A, Schuster D I, Blais A, Frunzio L, Huang R S, Majer J, Kumar S, Girvin S M and Schoelkopf R J 2004 *Nature* **431** 162
[13] Grajcar M *et al* 2004 *Phys. Rev.* B **69** 060501
[14] Johansson G, Tornberg L and Wilson C M 2006 *Phys. Rev.* B **74** 100504
[15] Filipp S *et al* 2009 *Phys. Rev. Lett.* **102** 200402
[16] Reuther G M, Zueco D, Hänggi P and Kohler S 2009 *Phys. Rev. Lett.* **102** 033602

[17] Reuther G M, Zueco D, Hänggi P and Kohler S 2011 *Phys. Rev.* B **83** 014303
[18] Bertet P, Chiorescu I, Burkard G, Semba K, Harmans C J P M, DiVincenzo D P and Mooij J E 2005 *Phys. Rev. Lett.* **95** 257002
[19] Bertet P, Chiorescu I, Harmans C J P M and Mooij J E 2005 Dephasing of a flux-qubit coupled to a harmonic oscillator arXiv:cond-mat/0507290
[20] Gardiner C W and Collett M J 1985 *Phys. Rev.* A **31** 3761
[21] Serban I, Plourde B L T and Wilhelm F K 2008 *Phys. Rev.* B **78** 054507
[22] Blais A, Huang R S, Wallraff A, Girvin S M and Schoelkopf R J 2004 *Phys. Rev.* A **69** 062320
[23] Mariantoni M, Deppe F, Marx A, Gross R, Wilhelm F K and Solano E 2008 *Phys. Rev.* B **78** 104508
[24] Leggett A J, Chakravarty S, Dorsey A T, Fisher M P A, Garg A and Zwerger W 1987 *Rev. Mod. Phys.* **59** 1
[25] Hänggi P, Talkner P and Borkovec M 1990 *Rev. Mod. Phys.* **62** 251
[26] Weiss U 1998 *Quantum Dissipative Systems* 2nd edn (Singapore: World Scientific)
[27] Makhlin Y, Schön G and Shnirman A 2001 *Rev. Mod. Phys.* **73** 357–400
[28] Ingold G L and Yu V Nazarov 1992 Charge tunneling rates in ultrasmall junctions *Single Charge Tunneling* (*NATO ASI Series B* vol 294) ed H Grabert and M H Devoret (New York: Plenum) pp 21–107
[29] Yurke B and Denker J S 1984 *Phys. Rev.* A **29** 1419
[30] Devoret M H 1995 *Quantum Fluctuations in Electrical circuits* (*Les Houches, Session LXIII*) (Amsterdam: Elsevier) chapter 10
[31] Makhlin Y and Mirlin A D 2001 *Phys. Rev. Lett.* **87** 276803
[32] Klimov A B and Sanchez-Soto L L 2000 *Phys. Rev.* A **61** 063802
[33] Klimov A B, Sainz I and Chumakov S M 2003 *Phys. Rev.* A **68** 063811
[34] Zueco D, Reuther G M, Kohler S and Hänggi P 2009 *Phys. Rev.* A **80** 033846
[35] Gardiner C W and Zoller P 2004 *Quantum Noise* 3rd edn (Berlin: Springer)
[36] Scofield J H 1994 *Am. J. Phys.* **62** 129
[37] Governale M, Grifoni M and Schön G 2001 *Chem. Phys.* **268** 273–83
[38] Fonseca-Romero K M, Kohler S and Hänggi P 2004 *Chem. Phys.* **296** 307
[39] Clerk A A, Devoret M H, Girvin S M, Marquardt F and Schoelkopf R J 2010 *Rev. Mod. Phys.* **82** 1155
[40] Lee J, Liu M and Wang H 2008 *IEEE J. Solid-State Circuits* **43** 1414
[41] Ojanen T and Salo J 2007 *Phys. Rev.* B **75** 184508
[42] Yamamoto T, Inomata K, Watanabe M, Matsuba K, Miyazaki T, Oliver W D, Nakamura Y and Tsai J S 2008 *Appl. Phys. Lett.* **93** 042510
[43] Chirolli L and Burkard G 2009 *Phys. Rev.* B **80** 184509
[44] Magalinskii V B 1959 *Zh. Eksp. Teor. Fiz.* **36** 1942
Magalinskii V B 1959 *Sov. Phys.—JETP* **9** 1381
[45] Benguria R and Kac M 1981 *Phys. Rev. Lett.* **46** 1
[46] Ford G W and Kac M 1987 *J. Stat. Phys.* **46** 803
[47] Hänggi P and Ingold G L 2005 *Chaos* **15** 026105
[48] Blum K 1996 *Density Matrix Theory and Applications* 2nd edn (New York: Springer)